Manifestation of anisotropy in melting systematics of RBa$_2$Cu$_3$O$_{7-\delta}$ (R=lanthanides)

H. B. Su[a)]
Division of Materials Science, Nanyang Technological University, 50 Nanyang Avenue, 639798 Singapore, Singapore

D. O. Welch[b)]
Department of Condensed Matter Physics and Materials Science, Brookhaven National Laboratory, Upton, New York 11973, USA

W. Wong-Ng,[c)] L. P. Cook, and Z. Yang
Ceramics Division, National Institute of Standards and Technology, Gaithersburg, Maryland 20899, USA

(Received 27 May 2007; accepted 25 September 2007; published online 24 October 2007)

The conventional isotropic Debye temperature fails to account for the trend of melting temperatures for the high T_c superconductors, RBa$_2$Cu$_3$O$_{7-\delta}$ (R-123), as a function of the ionic radius of R^{3+}. We overcame this problem by calculating Debye temperatures using mean sound velocity along the c axis that features an anisotropic layered structure. Using the "improved" Debye temperature, the trend of derived melting temperatures based on the "Lindemann law" matches well with experimental data. This trend is also confirmed by comparing theoretical and experimental Raman active modes corresponding to the Cu–O (plane copper and apical oxygen) and Ba–O (in-plane) bonds in R-123 series. © *2007 American Institute of Physics*. [DOI: 10.1063/1.2799242]

In recent years, there has been a growing interest in both bulk and multilayer RBa$_2$Cu$_3$O$_{7-\delta}$ (R-123, R=yttrium and lanthanides) cuprate superconductors,[1,2] particularly in coated-conductor applications.[3–6] To improve the properties and application range of R-123, prior knowledge of the phase stability of these compounds based on phase diagrams, including melting temperatures, is required. Understanding melting is important for both materials processing and for thermodynamic modeling. Osamura and Zhang[7] have systematically studied the change in melting temperature of R-123 superconductors (processed using "artificial air") as a function of the size r of R ions. Although a monotonic trend of melting temperature with r for the R-123 family has been experimentally observed, a detailed understanding of this trend at the atomic scale is not available due to the complexity of the structure of R-123. Poirier[8] found a correlation between the melting temperature and the Debye temperature for 15 compounds with the simple ABO_3 perovskite-type structure. This correlation stimulated us to carry out a systematic study of the dependence of melting temperature of R-123 on the ionic radius of R^{3+} or $r(R^{3+})$ based on the "Lindemann law."[9]

To confirm the melting trend with ionic size, as well as the variation of melting temperature of selected R-123 samples of interest under different atmospheric conditions, we prepared five R-123 samples (R=Nd, Sm, Gd, Y, and Er) using the solid-state technique. Stoichiometric amounts of $BaCO_3$, R_2O_3, and CuO were well mixed, and heat treated at 850 °C overnight. Subsequent heat treatments were conducted in air at 950 °C for 5 days with intermittent grindings. For the melting studies, two series of experiments were carried out using differential thermal/thermogravimetric analysis (DTA/TGA). Calibration of the system was completed using the α/β quartz transition (571 °C) and the melting points of NaCl and Au (801 and 1064 °C, respectively). In the first series, samples were annealed in oxygen to constant mass at 500 °C followed by slow cooling in oxygen to room temperature in order to ensure the maximum oxygen content of 7 in RBa$_2$Cu$_3$O$_{7-\delta}$.[10] Then DTA/TGA experiments were conducted in oxygen at 10 °C/min up to 1300 °C. In the second series of experiments, samples were also annealed in oxygen to constant mass at 500 °C followed by slow cooling, however the DTA/TGA experiments were conducted in purified air. We found that while the absolute values of the melting temperatures of these series of samples differ from each other, the general trends agreed well with each other, namely, the larger the size of R^{3+}, the higher the melting temperature. The difference in melting temperature for a given member of the series is due to the fact that melting temperature is higher under a higher oxygen partial pressure. These two sets of melting data are tabulated in Table I.

From thermodynamic considerations, the melting conditions of a compound can be obtained by equating temperatures, pressures, and Gibbs free energies of both solid and liquid phases. The traditional difficulty of such a thermodynamic melting theory arises from the complex relationship

TABLE I. Experimental melting temperatures of Ba$_2R$Cu$_3$O$_{7-x}$ measured under 0.1 MPa O$_2$ (or 100% O$_2$) and purified air. $r(R)^{3+}$ is the ionic radius (Å) of R^{3+} taken from Shannon by assuming a VIII-coordination environment (Refs. 13 and 14).

		Melting temperature	
R	$r(R)^{3+}$	0.1 MPa O$_2$ (or 100% O$_2$) °C (K)	purified air °C (K)
Sm	1.079	1097.0(1370.16)	1075.5(1348.66)
Eu	1.066	1089.6(1362.76)	1067.3(1340.46)
Gd	1.053	1069.7(1342.86)	1049.1(1322.26)
Y	1.019	1039.8(1312.96)	1021.0(1294.16)

[a)]Electronic mail: hbsu@ntu.edu.sg
[b)]Electronic mail: dwelch@bnl.gov
[c)]Electronic mail: winnie.wong-ng@nist.gov

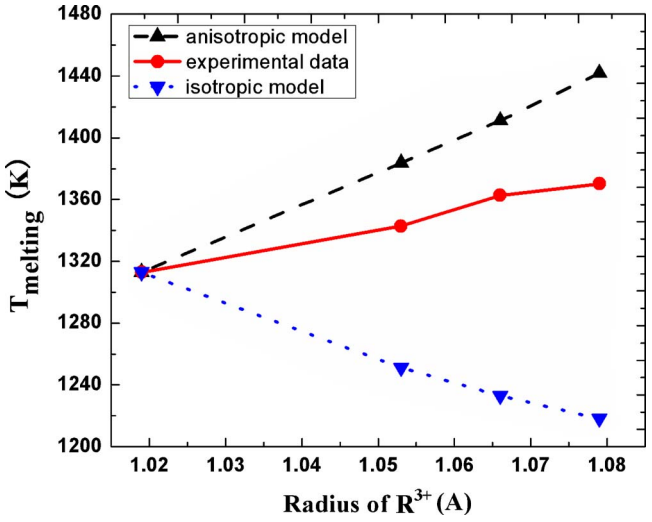

FIG. 1. (Color online) Calculated and experimental melting temperatures of $R\mathrm{Ba_2Cu_3O_7}$ as a function of $r(R^{3+})$ (Ref. 13 and 14). Solid circular symbols, linked by a solid read line, stand for experimental melting data under 0.1 MPa $p\mathrm{O_2}$ (100% $\mathrm{O_2}$). The data represented by down triangles, linked by a dot blue line, are calculated using the Debye temperatures by isotropic approximation. The data represented by up triangles, linked by a dash black line, are computed by selecting sound waves propagate along c axis.

between the free energy of the liquid phase and the interatomic forces. It is often necessary, especially for complex compounds, to resort to simple and conceptual methods, such as the Lindemann law.[9,11] The Lindemann theory assumes that at certain temperature the amplitude of vibration of solids is so large that the energy of the solid phase rises significantly. This temperature is the melting temperature of the solid. In 1950s, Gilvarry gave a firmer microscopic basis to the Lindemann law.[9] Instead of assuming that melting occurs when neighboring spheres collide, he stated that the root mean square amplitude of atomic vibrations at fusion r_m is a critical fraction of the distance of separation of nearest neighbor atoms. By substituting the root mean square amplitude of atomic vibration into Debye's approximation, we obtained the formula of melting temperature as

$$T_m = 0.0032 f^2 M V^{2/3} \Theta^2, \tag{1}$$

where M is the mean atomic mass of a solid, V is the mean atomic volume, f is the Gilvarry critical ratio, which is about 0.11 for perovskite oxides,[8] and Θ_D is the Debye temperature. If we simply proceed in this fashion using the Θ_D computed by an *isotropic* approximation, the calculated trend of melting temperature disagrees with the trend of measured data (Fig. 1). In order to explain the experimental results, it is necessary to examine carefully the structure of R-123 (see Fig. 1 in Ref. 20) and the elastic constants associated with the structure. There exists a notable anisotropic feature in this structure, namely, the elastic constants $[C_{33},(C_{44},C_{55})]$ are 50% smaller than $[(C_{11},C_{22}),C_{66}]$.[12] In fact, this layered structure can be approximated better by an anisotropic hexagonal model rather than the isotropic one. Note that the sound velocities are much smaller if the sound wave propagates along the c axis of the structure. If we calculate the Debye temperature by the mean sound velocity along the c axis, we can obtain better insight about melting since the vibrations along the c axis have larger amplitudes than those along the a and b axes. Hence, we first approximated the R-123 structure by a hexagonal one, then we computed the

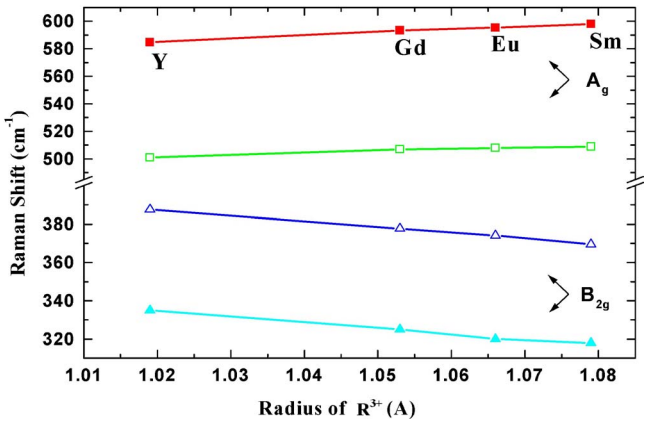

FIG. 2. (Color online) Raman Spectrum of $R\mathrm{Ba_2Cu_3O_7}$ as a function of radius of R^{3+}. Solid points stand for the calculated data; open ones for experimental data.[15] Squares are for A_g mode and triangles for B_{2g} mode.

sound velocities using a longitudinal/transverse wave along the c axis by

$$v_p = \sqrt{\frac{C_{33}}{\rho}},$$

$$v_s = \sqrt{\frac{C_{44}+C_{55}}{2\rho}}, \tag{2}$$

where ρ is the density. The mean sound velocity v_m can be computed by $3^{1/3}[(1/v_p^3)+(2/v_s^3)]^{-1/3}$. The Debye temperature is then given by

$$\Theta_D = \frac{h}{k_B}\left(\frac{3N_A}{4\pi V}\right)^{1/3} v_m, \tag{3}$$

where h is Planck's constant, k_B is the Boltzmann constant, N_A is Avogadro's number, and V is the molar volume. By using the melting temperature of Y-123 as a reference (scaling factor), the melting temperatures of the remaining R-123 were computed. Since the key feature, when comparing theoretical and experimental data, is strikingly similar for experimental data under both 100% $\mathrm{O_2}$ and purified air, we plotted only the computed data in Fig. 2 along with the current experimental melting data under 100% $\mathrm{O_2}$. The trend of the calculated melting temperatures agreed well with that of the experimental ones, although our calculated data were somewhat overestimated when compared with the experimental ones.

The trend of melting temperature dependence on $r(R^{3+})$ was corroborated by the calculations of selected Raman-active modes in $R\mathrm{Ba_2Cu_3O_7}$. We assessed the accuracy of our calculations by comparing the calculated and experimental A_g and B_{2g} Raman-active modes. The detailed calculation procedure of Raman modes was elaborated in Ref. 12. The A_g mode was assigned as the apical stretching mode due to the Cu–O bond (d_1) (planar copper and apical oxygen along the c axis). The B_{2g} mode is a result of an in-plane Ba–O stretching vibration. The frequency of the A_g mode [584^{calc} (503^{expt}) $\mathrm{cm^{-1}}$ for Y-123] and the B_{2g} mode [335^{calc} (388^{expt}) $\mathrm{cm^{-1}}$ for Y-123] were plotted, respectively, against $r(R^{+3})$ in R-123 (Refs. 13 and 14) in Fig. 2. The experimental data were taken from the work by Rosen *et al.*[15] The frequency of the Ag mode increases linearly with increasing $r(R^{+3})$ by approximately $2.28\%^{\mathrm{calc}}$ ($1.60\%^{\mathrm{calc}}$) from Y-123 to

Sm-123. At a first glance, this result appears to be inconsistent with the assignment of this mode to the apical oxygen bridging stretch vibration since the dimension of the unit cell in the c direction increases with increasing ionic radii. This expansion might be expected to lead to increasing bond lengths and decreasing force constants and therefore vibrational frequencies. However, neutron diffraction data show that despite the c axis increases, the Cu–O (d_2) (chain-copper and apical-oxygen) distances remain approximately constant[16] while the d_1 bond length decreases as the $r(R^{3+})$ increases.[13,14,16] Therefore the d_1 bond presumably controls the apical oxygen stretch frequency. The nice agreement between calculated and experimental d_1 bond lengths versus the $r(R^{3+})$ is shown in Ref. 12. On the other hand, the B_{2g} stretching mode [335^{calc} (388^{expt}) cm^{-1} for Y-123] decreases in frequency with increasing ionic radius. This change is substantial and corresponds to an approximately $4.64\%^{\text{calc}}$ ($-5.07\%^{\text{expt}}$) shift in the vibrational frequency. This shift is consistent with the identification of this mode as an in-plane Ba–O stretching vibration, since structural data indicate that the in-plane Ba–O bond lengths increase with the ionic radius of the rare earth.[12]

The sources of strain can be either host-lattice-nonconserved or host-lattice-conserved defects. One typical example for the former type is the strain field generated at R-123 grain boundaries, which strongly determines the segregation of calcium, consequently, affects passivating of disorder at the boundary.[17] Our work clearly demonstrates that the latter case, internal lattice strain, which occurs to accommodate the different ionic radii, has significant anisotropic effects on the trend of melting temperatures. As the ionic size of R increases, the distance of the Ba–O block between the barium layers becomes shorter along the c axis due to the shortening of the d_1 bond length. Due to the complexity of R-123 structure, one surprising consequence is that the corresponding *increase* of the separation between adjacent CuO_2 layers results in the remarkable reduction in the coherent interlayer single-particle hopping strength.[18] These results reveal the importance of the electronic origin of the rare-earth ionic anisotropic effect on T_c in this family.[19] In this study, this shortening in d_1 distance will increase the elastic constants $[C_{33},(C_{44},C_{55})]$ such that the melting temperature rises up with increasing ionic size of R. From previous studies,[20,21] it was found that while the formation energy of Schottky defects, which provides an unambiguous measure of the average cohesive strength (volumetric strain), is proportional to $B\Omega$ (where B is the bulk modulus and Ω is the mean volume per atom) for elemental and binary crystals; this relationship is violated in the R-123 series. In other words, the smaller the Schottky defect formation energy is, the lower is the melting temperature of simple elemental and binary crystals. Despite the fact that the Schottky defect formation energy of Sm-123 is smaller than that of Y-123, Sm-123 has the higher melting temperature, indicating that it is the internal strain due to the inhomogeneous changes of the bond distances within the unit cell for R-123 rather than the volumetric strain that controls the melting temperature of R-123. This intriguing finding is consistent with the melting systematics viewed from dislocation-mediated melting model, where the melting temperature is proportional to $B\Omega$ directly. The internal strains arising from the complex R-123 structure have significant anisotropic effects on the melting of these compounds. The dependence of melting temperatures on $r(R^{3+})$ that we report herein also provides a useful guide to estimate as well as to manipulate melting temperatures of $R\text{Ba}_2\text{Cu}_3\text{O}_{7-\delta}$ and of mixed lanthanide systems, $(R,R')\text{Ba}_2\text{Cu}_3\text{O}_{7-\delta}$.

Work at NTU is supported in part by COE-SUG grant (No. M58070001) and A*STAR SERC grant (No. 0521170032). The work at NIST was partially supported by the U.S. Department of Energy (DOE). The work at Brookhaven National Laboratory was performed under the auspices of the Division of Materials Sciences, Office of Science, U.S. Department of Energy under Contract No. DE-AC-02-98CH10886.

[1] A. Hu, M. Murakami, and H. Zhou, Appl. Phys. Lett. **83**, 1788 (2003).
[2] A. Hu, N. Sakai, and M. Murakami, Appl. Phys. Lett. **78**, 2539 (2001).
[3] A. P. Malozemoff, W. Carter, S. Flexhler, L. Fritzemeier, Q. Li, L. Masur, D. Parker, R. Parrella, E. Pedtburg, G. N. Riley, M. Rupich, J. Scudiere, and W. Zhang, IEEE Trans. Appl. Supercond. **9**, 2469 (1999).
[4] A. P. Malozemoff, S. Annavarapu, L. Fritzemeier, Q. Li, V. Prunier, M. Rupich, C. Thieme, W. Zhang, A. Goyal, M. Paranthaman, and D. F. Lee, Supercond. Sci. Technol. **13**, 473 (2000).
[5] A. Goyal, D. F. Lee, F. A. List, E. D. Specht, R. Feenstra, M. Paranthaman, X. Cui, S. W. Lu, P. M. Martin, D. M. Kroeger, D. K. Christen, B. W. Kang, D. P. Norton, C. Park, D. T. Verebelyi, J. R. Thompson, R. K. Williams, T. Aytug, and C. Cantoni, Physica C **357**, 903 (2001).
[6] T. Aytug, A. Goyal, N. Rutter, M. Paranthaman, J. R. Thompson, H. Y. Zhai, and D. K. Christen, J. Mater. Res. **18**, 872 (2003).
[7] K. Osamura and W. Zhang, Z. Metallkd. **84**, 522 (1993).
[8] J. P. Poirier, Phys. Earth Planet. Inter. **54**, 364 (1989).
[9] J. J. Gilvarry, Phys. Rev. **102**, 308 (1956).
[10] W. Wong-Ng, R. S. Roth, L. J. Swartzendruber, L. H. Bennett, C. K. Chiang, F. Beech, and C. R. Hubbard, *Ceramic Superconductors*, Advaced Ceramic Materials Vol. 2, edited by W. J. Smothers (American Ceramic Society, Westerville, OH, 1987), p. 565.
[11] J. P. Poirier, *Introduction to the Physics of the Earth's Interior* (Cambridge University Press, Cambridge, 1991).
[12] H. B. Su, Ph.D. thesis, State University of New York at Stony Brook, 2002.
[13] R. D. Shannon and C. T. Prewitt, Acta Crystallogr., Sect. B: Struct. Crystallogr. Cryst. Chem. **26**, 1046 (1970).
[14] R. D. Shannon, Acta Crystallogr., Sect. A: Cryst. Phys., Diffr., Theor. Gen. Crystallogr. **32**, 751 (1976).
[15] H. J. Rosen, R. M. Macfarlane, E. M. Engler, V. Y. Lee, and R. D. Jacowitz, Phys. Rev. B **38**, 2460 (1988).
[16] M. Guillaume, P. Allenspach, W. Henggeler, J. Mesot, B. Roessli, U. Staub, P. Fischer, A. Furrer, and V. Trounov, J. Phys.: Condens. Matter **6**, 7963 (1994).
[17] H. B. Su and D. O. Welch, Supercond. Sci. Technol. **18**, 24 (2005).
[18] E. Pavarini, I. Dasgupta, T. Saha-Dasgupta, O. Jepsen, and O. K. Andersen, Phys. Rev. Lett. **87**, 047003 (2001).
[19] X. J. Chen and H. B. Su, Phys. Rev. B **71**, 094512 (2005).
[20] H. B. Su, D. O. Welch, and W. Wong-Ng, Phys. Rev. B **70**, 054517 (2004).
[21] P. Varorsos and W. Ludwig, Phys. Rev. B **18**, 2683 (1978).